THE JOURNAL OF BIOLOGICAL CHEMISTRY VOL. 290, NO. 16, pp. 10242–10255, April 17, 2015

Targeted Ablation of the *Pde6h* Gene in Mice Reveals Cross-species Differences in Cone and Rod Phototransduction Protein Isoform Inventory*

Received for publication, September 18, 2014, and in revised form, March 2, 2015 Published, JBC Papers in Press, March 4, 2015, DOI 10.1074/jbc.M114.611921

Christina Brennenstuhl[‡], Naoyuki Tanimoto[§1], Markus Burkard[‡], Rebecca Wagner[‡], Sylvia Bolz[¶], Dragana Trifunovic[¶], Clement Kabagema-Bilan[‡], Francois Paquet-Durand[¶1], Susanne C. Beck[§], Gesine Huber[§], Mathias W. Seeliger[§], Peter Ruth[‡2], Bernd Wissinger[‖3], and Robert Lukowski[‡2,4]

From the Institute of Pharmacy, [‡]Department of Pharmacology, Toxicology and Clinical Pharmacy, [§]Division of Ocular Neurodegeneration, [¶]Division of Experimental Ophthalmology, and the [‖]Molecular Genetics Laboratory, Centre for Ophthalmology, University of Tuebingen, 72076 Tuebingen, Germany

Background: Phosphodiesterase-6 (PDE6) is a multisubunit enzyme essential for visual signal processing. Rare mutations in the human *PDE6H* gene result in incomplete color blindness.
Results: *Pde6h*-deficient mice exhibit no signs of photoreceptor dysfunction.
Conclusion: PDE6 configurations differ between species and are more interchangeable than previously thought.
Significance: Presence of related isoforms in the retina may allow adjustments of the phototransduction components thereby preventing the occurrence of pathological conditions.

Phosphodiesterase-6 (PDE6) is a multisubunit enzyme that plays a key role in the visual transduction cascade in rod and cone photoreceptors. Each type of photoreceptor utilizes discrete catalytic and inhibitory PDE6 subunits to fulfill its physiological tasks, *i.e.* the degradation of cyclic guanosine-3′,5′-monophosphate at specifically tuned rates and kinetics. Recently, the human *PDE6H* gene was identified as a novel locus for autosomal recessive (incomplete) color blindness. However, the three different classes of cones were not affected to the same extent. Short wave cone function was more preserved than middle and long wave cone function indicating that some basic regulation of the PDE6 multisubunit enzyme was maintained albeit by a unknown mechanism. To study normal and disease-related functions of cone *Pde6h in vivo,* we generated *Pde6h* knock-out (*Pde6h*$^{-/-}$) mice. Expression of PDE6H in murine eyes was restricted to both outer segments and synaptic terminals of short and long/middle cone photoreceptors, whereas *Pde6h*$^{-/-}$ retinae remained PDE6H-negative. Combined *in vivo* assessment of retinal morphology with histomorphological analyses revealed a normal overall integrity of the retinal organization and an unaltered distribution of the different cone photoreceptor subtypes upon *Pde6h* ablation. In contrast to human patients, our electroretinographic examinations of *Pde6h*$^{-/-}$ mice suggest no defects in cone/rod-driven retinal signaling and therefore preserved visual functions. To this end, we were able to demonstrate the presence of rod PDE6G in cones indicating functional substitution of PDE6. The disparities between human and murine phenotypes caused by mutant *Pde6h/PDE6H* suggest species-to-species differences in the vulnerability of biochemical and neurosensory pathways of the visual signal transduction system.

Transgenic and knock-out mouse models are widely used to study the physiology of phototransduction and the cellular mechanisms of vision impairment. In general, light detection in the murine and human retina follows the same principles, which involve two types of photoreceptors. At low light intensities visual cues are mainly detected by rods, whereas cones are important for color vision and vision at high light intensities (1, 2). Despite these differences in light sensitivities, photo-transduction in rods and cones involves related biochemical signaling pathways and a set of highly homologous but unique factors, including the different types of opsins, G-proteins, catalytic and regulatory subunits of phosphodiesterase-6 (PDE6), the various pore-forming and auxiliary subunits of the cGMP-gated cation channels (CNGs),[5] as well as proteins involved in phototransduction recovery such as opsin kinases, arrestins, membrane guanylate cyclases, *i.e.* GC-E and GC-F and GC-activating proteins (3–7).

The multisubunit enzyme PDE6 plays an essential role for the visual signal transduction process in both rods and cones; however, each type of photoreceptor utilizes discrete PDE6 subunits to fulfill its physiological tasks, *i.e.* the degradation of cyclic guanosine-3′,5′-monophosphate (cGMP) at specifically tuned rates and kinetics (8). Rod PDE6 is composed of two

* This work was supported by Deutsche Forschungsgemeinschaft Grants KFO134 and Ru573/5 (to P. R. and B. W.) and KFO134-Se837/5-2 and Se837/6-2 (to M. W. S.).
[1] Associates of Deutsche Forschungsgemeinschaft Research Unit 2060 (FOR2060) "cGMP Signaling in Cell Growth and Survival."
[2] Full members of the FOR2060.
[3] To whom correspondence may be addressed. Tel.: 49-7071-29-85032; Fax: 49-7071-29-5725; E-mail: bernd.wissinger@uni-tuebingen.de.
[4] To whom correspondence may be addressed. Tel.: 49-7071-29-74550; Fax: 49-7071-29-2476; E-mail: robert.lukowski@uni-tuebingen.de.

[5] The abbreviations used are: CNG, cGMP-gated cation channel; ACHM, achromatopsia; cd, candela; PNA, peanut agglutinin; GlyPhos, glycogen phosphorylase; OS, outer segment; IS, inner segment; SLO, scanning laser ophthalmoscopy; OCT, optical coherence tomography; ERG, electroretinogram; IF, immunofluorescence; L, long wavelength-sensitive; S, short wavelength-sensitive; M, medium wavelength-sensitive.

distinct PDE6α and PDE6β subunits that form a catalytic core encoded by the *Pde6a* and *Pde6b* gene, respectively. In the dark, the rod PDE6α/PDE6β heterodimer is inhibited by two identical γ-subunits (PDE6G) that are encoded by the *Pde6g* gene (9). In cone photoreceptors, PDE6 is formed by two identical PDE6α' subunits produced by the *Pde6c* gene and by two inhibitory PDE6γ' subunits (PDE6H), which derive from the *Pde6h* gene (10, 11).

Activation of PDE6 in rods and cones requires the Gα-subunits from the G-protein transducin ($G_t\alpha$), which upon light-induced release of $G_t\beta\gamma$ binds to PDE6 and thereby displaces the respective inhibitory γ-subunits (12). Light-induced activation of the different PDE6 multisubunit enzymes in photoreceptors results in a rapid drop in the intracellular concentration of cGMP and subsequently in closure of heterotetrameric CNG channels (3). In addition to many neuronal and cardiovascular functions of cGMP (13–15), cGMP binds to and activates CNG channels producing a stimulus-induced receptor potential. Ligand-dependent activation of photoreceptor CNG channels results in the so-called "dark current," a depolarizing current carried by a sustained entry of Na^+ and Ca^{2+} ions, which trigger neurotransmitter, *i.e.* glutamate release from photoreceptors as major synaptic input to bipolar cells.

Mutations in genes that code for proteins of the visual transduction system are a major cause of visual impairments (16). In this line, several studies report primary loss of proper PDE6 functions in photoreceptor pathology. Both the gene-targeted mouse model and humans revealed that defects in all so far identified genes encoding Pde6 subunits cause hereditary retinal diseases. For example, a mutation in the *Pde6b* gene produced an early onset retinal degeneration in the *rd1* mouse model (17). In humans, mutations in *PDE6B* cause autosomal dominant night blindness (18) or recessive retinitis pigmentosa (19) characterized by night blindness, initial rod photoreceptor degeneration, and gradual loss of vision leading to blindness (20). Similarly, mutations in the *PDE6A* and in the *PDE6G* genes were identified in several families with segregating autosomal recessive retinitis pigmentosa (21, 22). Accordingly, an ablation of the rod γ-subunit in gene-targeted *Pde6g* mice resulted in rapid retinal degeneration resembling human retinitis pigmentosa (23). We and others previously reported mutations in the human *PDE6C* gene encoding for the cone-specific catalytic PDE6α' subunits in patients that develop autosomal recessive inherited achromatopsia (ACHM) with early-onset cone photoreceptor dysfunction (24). Consistently, the *cpfl1* mutant mouse strain, which carries a spontaneous mutation in the *Pde6c* gene, develops pronounced cone dysfunction and photoreceptor degeneration (25). Likewise, mutations in the human genes for cone transducin α-subunit (*GNAT2*) (26), cone CNG channel (*CNGA3* and *CNGB3*) subunits (27), and *PDE6C* (24) as well as *PDE6H* (28) lead to autosomal recessive (incomplete) ACHM. Yet, important unresolved issues remained in case of the *PDE6H* mutation. In the three affected patients reported by Kohl and co-workers (28), a nonsense mutation within exon 2 of *PDE6H* was predicted to result in a truncated protein of only 11 amino acid residues lacking all conserved domains relevant for transducin binding (29, 30) and inhibition of the catalytic activity of PDE6. Because cone PDE6H includes 83 amino acid residues (11, 31), trichromatic color vision should be completely lost. However, S-cone function was more preserved than L- and M-cone function indicating that basic regulatory properties of the PDE6 multisubunit enzyme were maintained in S-cones by an unknown mechanism.

To elucidate the time course and mechanism(s) of cone degeneration triggered by loss of PDE6H function, we generated a *Pde6h*$^{-/-}$ mouse model that lacks the entire *Pde6h* locus. However, *Pde6h*$^{-/-}$ mice showed a normal retinal morphology, regular cone distribution, and unaltered retinal function in electroretinographic recordings despite the confirmed absence of cone PDE6H in *Pde6h*$^{-/-}$ mutant retinae. Evidence for the expression of the *Pde6g*-derived rod inhibitory subunit PDE6G in cones served as explanation of this unexpected phenotype. In contrast to humans, these results indicate that loss of *Pde6h* in dichromatic mouse retina can functionally be compensated by rod PDE6G. Together, the available evidence from previous reports (see Table 1) and this study reveal important species-to-species differences in their capabilities to respond to pathophysiological conditions of the visual transduction system.

EXPERIMENTAL PROCEDURES

Animal Welfare and Genetic Background—Experimental mice were bred and maintained at the animal facility of the Institute of Pharmacy, Department of Pharmacology, Toxicology and Clinical Pharmacy, University of Tübingen. All procedures concerning animals were performed with permission of local authorities and conducted in accordance with the German legislation on the protection of animals. The mice were kept in temperature- and humidity-controlled cabinets, in a standard 12-h light-dark cycle with *ad libitum* access to food and water. For the experiments, global *Pde6h* knock-out mice (genotype *Pde6h*$^{-/-}$) were compared with age or age- and litter-matched wild-type mice (genotype *Pde6h*$^{+/+}$) on a hybrid SV129/C57BL/6 genetic background. Animals were used irrespective of their gender at an age of 12–52 weeks.

Generation of the Pde6h-deficient Mouse Model—The *Pde6h* homology arm fragments for the assembly of the targeting construct were taken from a bacterial artificial chromosome isolated from a 129/Sv mouse bacterial artificial chromosome library (RZPD, Berlin, Germany). The targeting vector contained a *Neo/Tk* selection cassette flanked by two loxP sites located downstream of exon 4 and a single loxP site together with a new SpeI restriction site (for subsequent identification of the homologous recombination by Southern blot analysis) in intron 2. Therefore, the entire protein coding exons 2–4 of the *Pde6h* gene were flanked by two loxP sites (Fig. 1*A*). R1 embryonic stem (ES) cells were electroporated with the linearized targeting construct and screened for G418-resistant clones. Homologous recombination was confirmed by Southern blot analysis upon HindIII- and SpeI-digested ES cell DNA. One correctly targeted clone (L3/+) was injected into C57BL/6 blastocysts. The resulting chimeras were mated with C57BL/6 mice to obtain germ line transmission, resulting in heterozygous *Pde6h*$^{L3/+}$ offspring. *Pde6h*$^{L3/+}$ mice were crossed to Cre deleter animals (genotype CMV-Cre$^{tg/0}$) (32) to excise the coding exons of *Pde6h* and the *Neo/Tk* cassette. This produced double

transgenic animals with the desired *Pde6h*$^{-/+}$; CMV-Cre$^{tg/0}$ genotype. *Pde6h*$^{-/+}$; CMV-Cre$^{tg/0}$ mice were then backcrossed to C57BL/6 mice to eliminate the Cre transgene. Heterozygous offspring (genotype *Pde6h*$^{-/+}$) were intercrossed to establish homozygous *Pde6h*-deficient mice (*Pde6 h*$^{-/-}$) and littermate control animals for the experiments. Animals were genotyped by PCR using mouse tail genomic DNA with three primers (F1, 5′-TCCATGTGAACAGGGAGCCAG-3′; F2, 5′-CGATGTGAGCTTAGGGCTCTG-3′; and R, 5′-GCCTTCCCTACCCATCCTC-3′) that amplified either the WT (446 bp) or the *Pde6h* knock-out allele (346 bp) (Fig. 1*D*).

Immunoblotting of Proteins from Mouse Retina and of Recombinant PDE6H Protein—For protein extraction from pooled mouse retinae ($n = 4–6$ per genotype), enucleated eyes were homogenized mechanically (Ultra-Turrax) in homogenization buffer (20 mM Tris-HCl (pH 8.3), 0.67% SDS, 238 mM β-mercaptoethanol, 0.2 mM PMSF). Western blot analysis was performed according to a previously established protocol (33–35). As a positive control, a PDE6H-hexahistidine fusion protein was loaded together with the protein samples derived from *Pde6h*$^{-/-}$ and WT retina. For heterologous recombinant expression of the tagged PDE6H protein in *Escherichia coli*, the complete coding sequence of the mouse *Pde6h* cDNA was cloned into the pQE81 plasmid. The resulting PDE6H-hexahistidine fusion protein was induced by isopropyl 1-thio-β-D-galactopyranoside (1 mM) and purified by an imidazole gradient separation on nickel-nitrilotriacetic acid columns as recommended by the manufacturer's instructions (Qiagen, Hilden, Germany). Extracted proteins were separated by their molecular weight using denaturing SDS-17.5% PAGE. Immunodetection was performed according to standard procedures using primary antibodies detecting PDE6G/H (1:250 dilution; Santa Cruz Biotechnology, Dallas), PDE6H (1:1000 dilution), and p42/p44 MAPK (1:1000 dilution; Cell Signaling Technology, Cambridge, UK). To identify the primary antibody protein complexes, a secondary anti-mouse Cy3 antibody and an anti-rabbit Cy5 antibody (1:2500 dilution; Santa Cruz Biotechnology) were used. An Ettan DIGE System (GE Healthcare) was used to detect the fluorophores.

Primary Retinal Single Cell Cultures—Eyeballs from euthanized mice were enucleated, and the cornea, lens, vitreous body, and sclera were removed. The remaining retina was transferred to 300 μl of digestion buffer containing 960 μg/ml papain, 9.8 μg/ml BSA, and 9.8 mM DTT in Ca^{2+}-free buffer. To achieve complete dissociation, the tissue was digested for 10 min at 37 °C, then triturated 3–5 times using a 1000-μl pipette tip, and further digested for 5 min at 37 °C followed by a second trituration step. 2 μl of DNase I working solution (Sigma) were added for 5 min at 37 °C to the dispersed retina, and a final trituration was performed using a cannula (0.3 × 13 mm) to obtain the cell suspension. Papain activity was stopped by transferring the single cell solution to 1.5 ml of cell culture medium (45% Ham's F-12, 45% DMEM, 10% FCS; containing 2 mM L-glutamine, 10 mM HEPES, and 10 ml/liter penicillin/streptomycin (Biochrom, Berlin, Germany)). After a single centrifugation step at 2000 rpm for 5 min, the pellet was resuspended again in cell culture medium, and 150–200 μl of the suspension were plated on glass slides coated with poly-D-lysine/PBS (1:100; Sigma) equipped with μ-Chambers (ibidi, Martinsried, Germany). Single cell cultures of the retina were incubated at 37 °C for 30 min at maximum. Subsequently, the cells were fixed with 2% paraformaldehyde in PBS for 5 min, washed with PBS, and stored at 4 °C until immunofluorescence staining was performed.

Immunofluorescence of Retinal Sections and Primary Retinal Single Cell Cultures—Mouse, rat, and bovine eyes were enucleated; eyecups were dissected, rinsed with PBS, and fixed overnight in 2% paraformaldehyde in PBS, dehydrated successively in an alcohol series of ethanol, and then embedded in paraffin. Sectioning was performed in 8-μm intervals. Retina slices were deparaffinized and rehydrated in an alcohol series followed by permeabilization with 0.3% Triton X-100/PBS, as described previously (36).

For immunofluorescence (IF) staining, retinal sections or cultured retina-derived single cell cultures were washed with PBS, blocked with 5% normal goat serum in PBS for 1 h, and incubated overnight at 4 °C in primary antibody dilutions. The primary antibodies used for the IF were specific for PDE6H (1:1000 dilution; as described previously (28)), PDE6G/H (1:1000 dilution; Santa Cruz Biotechnology), glycogen phosphorylase (1:1000 dilution (37–39)), and peanut agglutinin (PNA) conjugated to FITC or Alexa 568 (1:100 dilution, Sigma). Detection of the primary antibody-antigen complexes was carried out by appropriate Cy2- or Cy3-conjugated secondary antibodies (1:200 dilution, Dianova, Hamburg, Germany) and mounted in PermaFluor (Thermo Fisher Scientific, Waltham) containing 1 μg/ml Hoechst (Sigma) for the nuclear counterstain. Axio-imager Z1 or ApoTome fluorescence microscopes (Zeiss, Oberkochen, Germany) were used to examine the IF.

Digital quantification of the PDE6H or PDE6G/H fluorescence in *Pde6h*$^{-/-}$ and WT retina was performed in optical slices double-stained for PNA-FITC and PDE6H or PNA-FITC and PDE6G/H. Quantitative analyses of fluorescence intensities at defined coordinates were measured in grayscales using the Axiovert software for profile measurement in the ApoTome modus. Analysis was performed for 20 PNA-positive cone outer segments in retinal slices derived from *Pde6h*$^{-/-}$ and WT mice. All data were normalized against the corresponding background fluorescence.

Histology of Retinal Fine Structure and Whole Mount Immunohistochemistry—For the histological assessment, 8-μm sections of paraffin-embedded retina were used. Hematoxylin and eosin staining (H&E) was performed according to a previously published protocol. Digital images were obtained by the use of an Axio Cam MRc attached to an Axiovert 200 M microscope (Zeiss).

For retinal whole mount staining, eyecups were dissected, and the orientation of the retina was marked by a small incision. Isolated retinae were flat-mounted on slides, fixed for 40 min with 2% paraformaldehyde, transferred onto a filter paper with the photoreceptor layer up, and kept in 0.1 M phosphate buffer. Whole mounts were washed in 0.1 M phosphate buffer and blocked with 5% ChemiBLOCKER (EMD Millipore Billerica) containing 0.5% Triton X-100 and 0.05% NaN_3 for 1 h. Primary antibodies were applied overnight at 4 °C. After several washing steps, whole mounts were sealed in Vectashield to prevent photobleaching.

In Vivo Electroretinography—Full-field electroretinograms (ERGs) were recorded from Pde6h$^{-/-}$ and WT littermate mice at an age of 4–5 months according to the procedures described

previously (40). In brief, mice were dark-adapted overnight before the experiments and anesthetized with a subcutaneous injection of a mixture of ketamine (66.7 mg/kg body weight) and xylazine (11.7 mg/kg body weight). The pupils were dilated, and single-flash ERGs were obtained under dark-adapted (no background illumination, 0 cd/m^2) and light-adapted (with a background illumination of 30 cd/m^2 starting 10 min before recording) conditions. Single white-flash stimuli ranged from −4.0 to 1.5 log cd s/m^2 under dark-adapted and from −2.0 to 1.5 log cd s/m^2 under light-adapted conditions. Ten responses were averaged with inter-stimulus intervals of 5 s (for −4 to −0.5 log cd s/m^2) or 17 s (for 0–1.5 log cd s/m^2). Responses to trains of brief flashes (flicker) for a fixed intensity (0.5 log cd s/m^2) with 12 frequencies (0.5, 1–3, 5, 7, 10, 12, 15, 18, 20 and 30 Hz) were obtained without any background illumination (0 cd/m^2), which were averaged either 20 times (for 0.5 to 3 Hz) or 30 times (for 5 Hz and above). Bandpass filter cutoff frequencies were 0.3 and 300 Hz for all ERG recordings. ERG data were recorded from four WT and four *Pde6h*$^{-/-}$ animals.

Scanning Laser Ophthalmoscopy and Optical Coherence Tomography—Scanning laser ophthalmoscopy (SLO) and spectral domain optical coherence tomography (OCT) imaging were done in the same session as the ERGs in *Pde6h*$^{-/-}$ and WT. SLOs and OCTs were obtained as reported previously (41, 42).

Scanning laser ophthalmoscopy was performed with a Heidelberg Retina Angiograph (HRA I, Heidelberg Engineering, Germany). The HRA features two argon wavelengths (488 and 514 nm) in the short wavelength range and two infrared diode lasers (795 and 830 nm) in the long wavelength range. Laser wavelengths used for fundus visualization were as follows: 830 nm (infrared channel) and 514 nm (red-free channel). Additionally, the 488- and 795-nm lasers were used for fluorescein and indocyanine green angiography, respectively. Fluorescein angiography was performed using an s.c. injection of 75 mg/kg body weight sodium fluorescein (University Pharmacy, University of Tübingen, Germany) and indocyanine green angiography following an s.c. injection of 50 mg/kg body weight indocyanine green (ICG-Pulsion, Pulsion Medical Systems AG, Munich, Germany). SD-OCT imaging was performed with a Spectralis^{TM} HRA + OCT device from Heidelberg Engineering featuring a broadband superluminescent diode as low coherent light source (43). Each two-dimensional B-scan recorded with the equipment set to 308 fields of view consists of 1536 A-scans acquired at a speed of 40,000 scans/s. Optical depth resolution is 7 μm with digital resolution reaching 3.5 mm. Image data were analyzed using the proprietary software package Eye Explorer from Heidelberg Engineering.

RESULTS

Generation of Pde6h$^{-/-}$ *Mice*—To define the role of the inhibitory subunit of cone phosphodiesterase-6 for photoreceptor function *in vivo*, we generated mice lacking a functional *Pde6h*. Exons 2–4, which include the entire protein coding sequences of murine *Pde6h*, were flanked with two loxP sites and a *Neo/TK* selection cassette by homologous recombination (Fig. 1*A*). ES cells were screened for correct targeting by Southern blot analysis (Fig. 1*B*). The integrity of the loxP sites was tested *in vitro* using L3/+ ES cells that were subjected to a transient expression of the Cre recombinase. As expected, this second targeting resulted in ES cells that were either heterozygous for the conditional (L2) or null (L1 or −) allele of *Pde6h* (Fig. 1, *A* and *C*). To establish a conditional and constitutive knock-out mouse line, we used one correctly targeted L3/+ clone for the blastocyst injection and generated four chimeric mice, two of which showed germ line transmission of the L3/+ allele. We obtained heterozygous *Pde6h*-deficient (*Pde6h*$^{+/-}$) progenies by mating the germ line founders, which carried the targeted *Pde6h* allele (*Pde6h*$^{L3/+}$) with a transgenic Cre-deleter mouse line (Fig. 1*D*) (32). Offspring heterozygous for the targeted *Pde6h* allele were subsequently backcrossed to C57BL/6 mice to obtain heterozygous *Pde6h*$^{+/-}$ animals that lost the Cre recombinase transgene. Intercrossing of *Pde6h*$^{+/-}$ mice yielded age- and litter-matched *Pde6h*$^{-/-}$ knock-out and WT (genotype *Pde6h*$^{+/+}$) animals at the expected Mendelian ratios (Fig. 1*D*). *Pde6h*$^{+/-}$ and *Pde6h*$^{-/-}$ mice were viable and fertile and did not show any gross abnormalities confirming that the *Pde6h* gene is not essential for a normal pre- and postnatal development.

Lack of the PDE6H Protein from Retinal Cone Photoreceptor Cells in Pde6h$^{-/-}$ *Mice*—To verify the retinal distribution of PDE6H on a cellular level and to confirm the absence of the PDE6H protein in the *Pde6h*$^{-/-}$ model, we first investigated retinal cryosections and primary retinal cell cultures obtained from WT and *Pde6h*$^{-/-}$ mice. Immunofluorescence staining was performed by using in-house-generated antibodies that were either specific for PDE6H or glycogen phosphorylase (GlyPhos), a widely used cone-specific marker. As in previous studies (28), the co-localization experiments in WT retina showed that the PDE6H protein was exclusively located in cone photoreceptors and not present in any other retinal cell type. The highest PDE6H intensities were detected in cone outer segments (OS), whereas inner segments (IS) and synaptic terminals of cone photoreceptors showed a weaker (but consistent) staining. Retinal sections of *Pde6h* null mice remained PDE6H-negative confirming efficient deletion of the *Pde6h* gene in the KOs (Fig. 2*A*). Interestingly, we observed a normal cellular morphology and layering of *Pde6h*-deficient retinae that were obtained from young and old mice, *i.e.* about 52-week-old mice indicating that the lack of PDE6H protein does not cause a loss of photoreceptor cells neither during development nor as a result of a postnatal progressive degenerative process.

To discriminate exactly between rod and cone expression of PDE6H, we analyzed enzymatically dissociated murine retina. In these cultures, the different types of photoreceptors can be well discriminated from any other retinal cell types. Primary cells derived from *Pde6h*$^{-/-}$ and WT retinae were plated and analyzed by immunofluorescence staining using the above-mentioned antibodies against PDE6H and GlyPhos. These co-localization experiments revealed that PDE6H was present in all GlyPhos-positive cells from dispersed WT retinae, whereas GlyPhos-positive cells from *Pde6h*$^{-/-}$ retinae could not be labeled for PDE6H (Fig. 2*B*). Importantly, the primary cells confirmed that the PDE6H protein was restricted to cone photoreceptors because we never observed PDE6H in GlyPhos-nega-

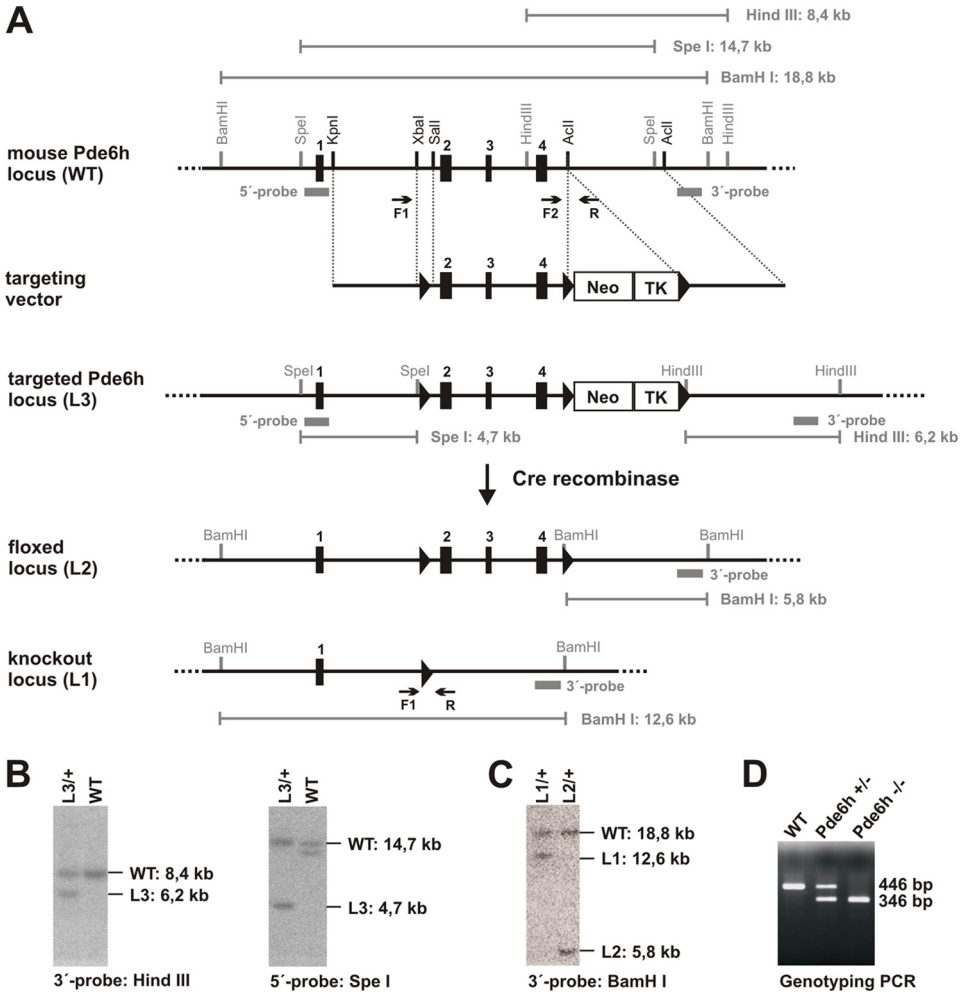

FIGURE 1. **Targeted deletion of the murine *Pde6h* gene using the Cre/loxP system.** *A*, targeting strategy. *Top,* murine WT *Pde6h* gene locus and targeting vector containing a *Neo/Tk* cassette flanked by two loxP sites (*black triangles*) downstream of the coding exons 2–4 and a single loxP site upstream of exon 2. *Middle,* targeted allele (L3) after neomycin (*Neo*) selection. *Bottom,* treatment of a targeted allele with Cre recombinase and subsequent negative selection using gancyclovir, which is toxic in the presence of thymidine kinase (*Tk*) yielded a modified *Pde6h* allele where the coding exons are flanked by two loxP sites (L2) or a null allele with a deletion of all coding exons (L1). Diagnostic restriction sites, *i.e.* HindIII, SpeI, and BamHI as well as the position of all probes for the Southern analysis (*gray bars*), are indicated. *Black arrows* indicate the position of the PCR primers used to identify the different *Pde6h* alleles. *B*, first targeting, representative ES cell Southern blots. To verify the correct integration of the 3′-homology arm, genomic ES cell DNA was digested with HindIII and hybridized with the 3′-probe yielding an 8.4- and a 6.2-kb fragment representing the WT and the targeted L3 allele (*left*). To analyze the correct integration of the 5′-homology arm, genomic ES cell DNA was digested with SpeI and hybridized with the 5′-probe yielding a 14.7- and a 4.7-kb fragment representing the WT and the targeted L3 allele (*right*). *C*, Southern blot of L3 ES cells after transfection with Cre recombinase. DNA was digested with BamHI and hybridized with the 3′-probe yielding 18.8-, 12.6-, and 5.8-kb fragments representing the WT, null (L1), and conditional knock-out allele (L2), respectively. *D*, PCR genotyping of murine tail tip DNA from WT, heterozygous (*Pde6h*$^{+/-}$), and *Pde6h*$^{-/-}$ animals using specific primers F1, F2, and R (*arrows* in *A*). The size of the expected amplicons is 446 bp for WT and 346 bp for the knock-out allele, respectively.

tive cells (data not shown). Together, our present findings are in good agreement with previous reports (11) implying that the retinal expression of PDE6H in the eye is indeed restricted to cone photoreceptors.

We next examined the distribution of the PDE6H protein in rat and bovine retina (Fig. 2*C*). In rat retina, highest PDE6H intensities were observed in the cone photoreceptor IS. Similarly, PDE6H protein in bovine retina was more concentrated to the IS than the OS. Immunoreactivity for PDE6H appeared to be high in the base region of the bovine cone OS, whereas in the distal portion of the OS much less PDE6H was detectable.

Normal Retinal Morphology, Cone Subtype Distributions, and Photoreceptor Densities in Pde6h$^{-/-}$ *Mice*—Because the genetic ablation of the catalytic *Pde6* subunits in both cones or rods and of the rod-specific γ-subunit of PDE6 in mice caused prominent histological changes, including photoreceptor degeneration, and result in severe functional defects of the retina (21–25, 28), we performed a combined histomorphological and cone distribution study in our *Pde6h*$^{-/-}$ mouse model.

Pde6g null mice that carry a deletion of the inhibitory γ-subunit of rod PDE6 exhibit a severe and progressive loss of photoreceptor cells leading to early retinal degeneration (23). In contrast, hematoxylin and eosin staining of retinal paraffin sections from young (data not shown) and old *Pde6h*$^{-/-}$ animals did not show any obvious morphological abnormalities, *i.e.* neither the overall structure of the retina nor its organization into the typical layers were altered by the lack of the PDE6H protein (Fig. 3*A*). Next, we performed an IF analysis on whole mount staining obtained from *Pde6h*$^{-/-}$ and WT retina using two different antibodies directed against M- or S-opsins, respectively.

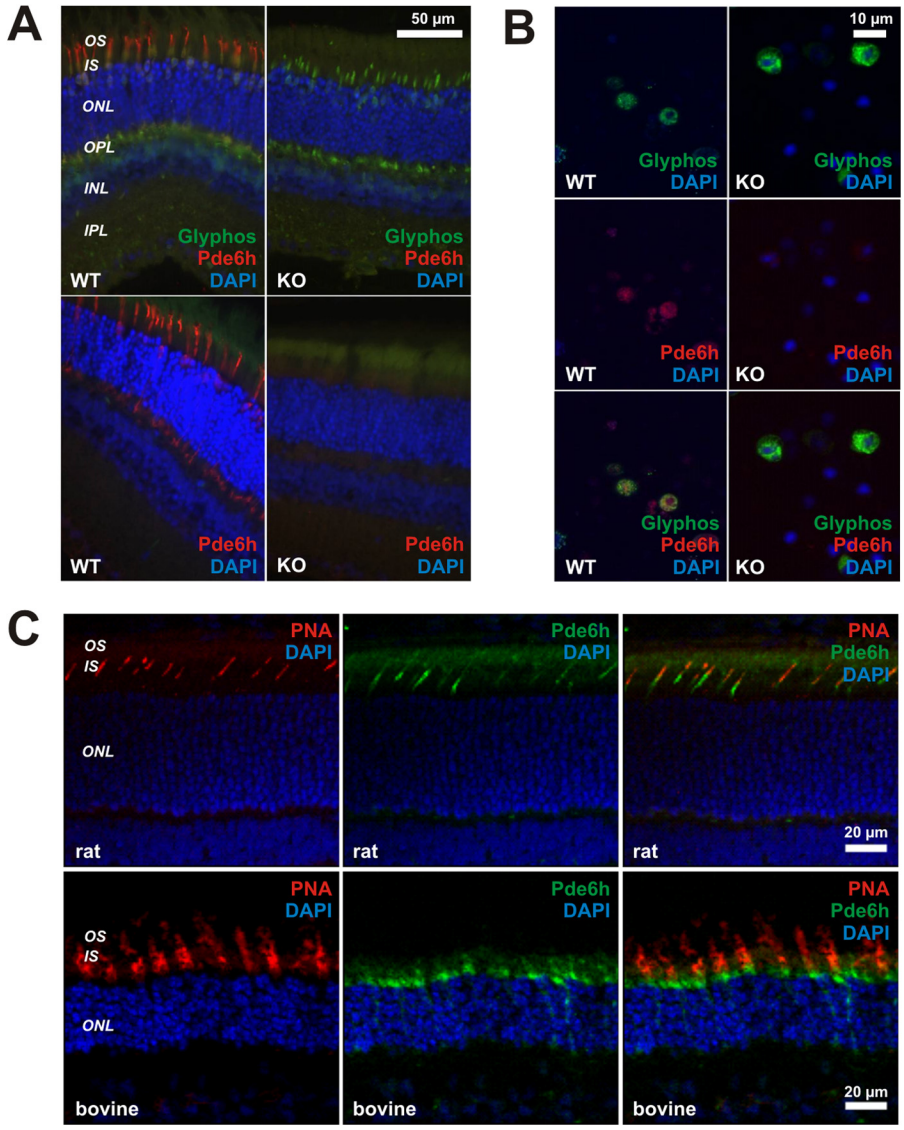

FIGURE 2. **Analysis of PDE6H protein expression in rat, bovine, and murine retinal slices and in primary retinal cell culture from WT and *Pde6h*$^{-/-}$ mice.** *A,* PDE6H immunofluorescence in retina of WT and *Pde6h*$^{-/-}$ (KO) mice labeled for PDE6H (*red*, 1:1000) and for GlyPhos (*green*, 1:1000) as a cone marker. *INL*, inner nuclear layer; *IPL*, inner plexiform layer; *IS*, photoreceptor inner segments; *ONL*, outer nuclear layer; *OPL*, outer plexiform layer; *OS*, photoreceptor outer segments. *B,* immunofluorescence analysis of PDE6H expression in primary retinal cell culture from WT and *Pde6h*$^{-/-}$ mice. Single retina cells were co-labeled for PDE6H (*red*, 1:1000) and GlyPhos (*green*, 1:1000). Single channel (*upper, middle*) and multichannel (*lower*) panels are shown. The immunofluorescence staining in *A* and *B* confirmed that PDE6H protein is present in cone photoreceptors of WT mice but absent from *Pde6h*$^{-/-}$ cones. DAPI was used as a nucleus-staining fluorochrome. *C,* PDE6H immunofluorescence in rat and bovine retina. Sections were co-labeled for PDE6H (*green,* 1:1000) and peanut hemagglutinin (PNA-Alexa568, *red*, 1:100) as cone marker. *INL,* inner nuclear layer; *OPL,* outer plexiform layer; *ONL,* outer nuclear layer; *OS,* photoreceptor outer segments.

Surprisingly, we did not observe any differences in the distribution of M-opsin- (Fig. 3*B*) and S-opsin-expressing cones (Fig. 3*C*) in ventral and dorsal parts of the retina between both genotypes. The nonhomogeneous distribution of S-opsin expression in *Pde6h*$^{-/-}$ and in WT retinae, *i.e.* a high number of S-opsin-expressing cones in the ventral part and a low abundance in the dorsal part of the retina represent the physiological distribution in mice and correlate well with previous reports (44, 45). From our recent analysis of three human patients that carry a mutation in *PDE6H* (28), we expected that M-cone (and M-/S-cone) functions and therefore their numbers would be affected in the *Pde6h* null retina. However, on the histomorphological level, we did not find any signs for M- or S-cone degeneration (Fig. 3*B*). These histological investigations were corroborated by an *in vivo* assessment of the retinal morphology using SLO imaging and OCT.

In vivo SLO en face fundus imaging (Fig. 3*D*) as well as angiography (data not shown) demonstrated normal fundus appearance and normal retinal vasculature, respectively. Analysis of retinal morphology with *in vivo* OCT imaging demonstrated regular retinal thickness and normal retinal layering (Fig. 3*E*), suggesting, together with the histomorphological examinations (Fig. 3, *A*–*C*), that *Pde6h* is dispensable for retinal integrity and the proper organization of cone photoreceptors.

Ablation of Pde6h Does Not Alter Mouse Cone and Rod Photoreceptor Functions—To assess whether the lack of *Pde6h* has consequences for photoreceptor functions, full-field single-flash ERGs were recorded from *Pde6h*$^{-/-}$ and WT littermates

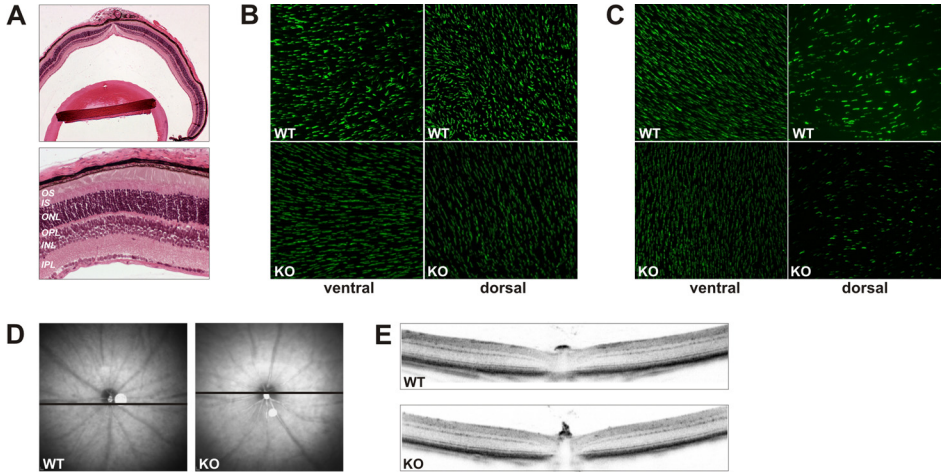

FIGURE 3. **Retinal morphology in *Pde6h*$^{-/-}$ mice.** *A*, representative overview image (*top*) of a *Pde6h*$^{-/-}$ retina stained with hematoxylin and eosin (*H&E*) and higher magnification (*bottom*) reveal normal retinal morphology. *IPL,* inner plexiform layer; *INL,* inner nuclear layer; *OPL,* outer plexiform layer; *ONL,* outer nuclear layer; *IS,* photoreceptor inner segments; *OS,* photoreceptor outer segments. *B*, comparison of M-opsin expression pattern in retinal whole mount staining of WT (*top*) and *Pde6h*$^{-/-}$ (*bottom,* KO) mice representing ventral and dorsal retinal fields. *C*, comparison of S-opsin expression pattern in retinal whole mount staining of WT (*top*) and *Pde6h*$^{-/-}$ (*bottom*, KO) mice representing ventral and dorsal retinal fields. No differences in M- or S-opsin expression between the both groups were observed. *D*, representative examples of retinal SLO en face imaging in WT (*left*) and *Pde6h*$^{-/-}$ mice (right, KO). The *black bars* in *D* indicate the virtual section plane for OCT data in *E*. *E*, OCT data in WT (*top*) and *Pde6h*$^{-/-}$ (*bottom,* KO) mice. SLO and OCT analysis revealed no differences between WT and *Pde6h*$^{-/-}$ retinae.

under both dark-adapted and light-adapted conditions (Fig. 4, *A* and *B*). The initial negative-deflecting a-wave that appears at middle and high intensities is initiated by photoreceptors. The so-called b-wave, a large positive deflection that follows the a-wave, mainly includes ON-bipolar cell activity and hence represents signaling downstream of the photoreceptors. Because the input to bipolar cells is derived from the preceding photoreceptor cells, the b-wave indirectly also reflects the activity of rods and cones and is a practical indicator for photoreceptor-ON-bipolar cell functionality. In contrast to the ERG phenotype of the three human patients that carry a stop mutation in the *PDE6H* gene (28), dark-adapted and light-adapted single-flash ERGs of WT and *Pde6h*$^{-/-}$ mice appeared similar in size and shape (Fig. 4, *A*, *B* and *D*), and we could not detect any difference in b-wave amplitudes (Fig. 4*C*). These results suggest that the deletion of *Pde6h* in mice does not affect rod- or cone-dependent ON-bipolar cell signaling. By recording ERGs during a flicker stimulation (Fig. 4, *E* and *F*), we further obtained some additional information about cone ON- and OFF-pathway signaling in *Pde6h*$^{-/-}$ mice. In this flicker frequency series, the stimulus intensity remains the same at 0.5 log cd s/m^2, whereas stimulus frequency is increased stepwise from 0.5 to 30 Hz without any adapting background illumination. Under the given conditions, the flicker responses are dominated by activity in the rod system below 5 Hz, cone ON-pathway between 5 and 15 Hz, and cone OFF-pathway above 15 Hz (46). At all applied stimulus frequencies, there was no remarkable difference in flicker responses between WT and *Pde6h*$^{-/-}$ mice (Fig. 4, *E* and *F*). Together, the ERG measurements suggest no defects in cone-driven or rod-driven retinal signaling and that overall retinal function is not impaired in *Pde6h*$^{-/-}$ mice.

Cone Photoreceptor Cells in Pde6h$^{-/-}$ *Mice Express the Rod Pde6g Homolog*—In contrast to the three patients with homozygous nonsense mutations in *PDE6H*, our *in vivo* ERG analysis revealed that *Pde6h*$^{-/-}$ mice neither exhibit reduced cone functions nor absent flicker responses indicative for a homologous phenotype (28). We therefore reasoned that an ablation of the entire *Pde6h* gene in dichromatic mouse retina would be compensated by a mechanism that maintains a regular light-evoked signal processing from cones to bipolar cells. We first tested whether an unexpected presence of the PDE6G protein (the rod isoform of PDEγ) in *Pde6h*$^{-/-}$ cones was responsible for a preserved regulation of the catalytic subunits of PDE6. FITC-linked PNA was used as cone marker on mouse WT and *Pde6h*$^{-/-}$ retinal sections for co-labeling experiments with antibodies specifically detecting either the PDE6H protein (Fig. 5*A*) or both homologs *i.e.* PDE6G and PDE6H (Fig. 5, *C* and *D*).

In agreement with our previous results obtained from co-labeling of cone photoreceptors with GlyPhos antibodies (Fig. 2, *A* and *B*), we observed high expression of PDE6H in the outer segments of PNA-FITC-labeled cones of the WT retina, whereas photoreceptors from *Pde6h* null mice remained PDE6H-negative (Fig. 5*A*). As expected, the PDE6G/H common antibody homogeneously labeled the entire photoreceptor layer, including the PNA-FITC-positive cones of WT retina (Fig. 5*C*). By using the same PDE6G/H common antibody, we observed a highly analogous staining pattern in *Pde6h*$^{-/-}$ retina (Fig. 5*C*), *i.e.* co-staining of PNA-FITC-tagged cones with the PDE6G/H common antibody. Because we repeatedly confirmed full ablation of the PDE6H protein in the *Pde6h*$^{-/-}$ mouse model, this finding points to the presence of PDE6G in *Pde6h*$^{-/-}$ cones.

To avoid superimposing fluorescence signals from rod to cones, we digitally measured and quantified relative fluorescence intensities in optical sections devoid of scattered light and upon background subtraction in WT and *Pde6h*$^{-/-}$ (Fig. 5, *B*, *D*, and *E*). Again, PNA-FITC fluorescence was used to detect cone outer segments (peak of green fluorescence; *arrows* in Fig. 5*D*). Subsequently, corresponding PDE6H or PDE6G fluorescence intensities at the same coordinates, obtained by labeling of the retina with PDE6H or PDE6G/H antibodies, were deter-

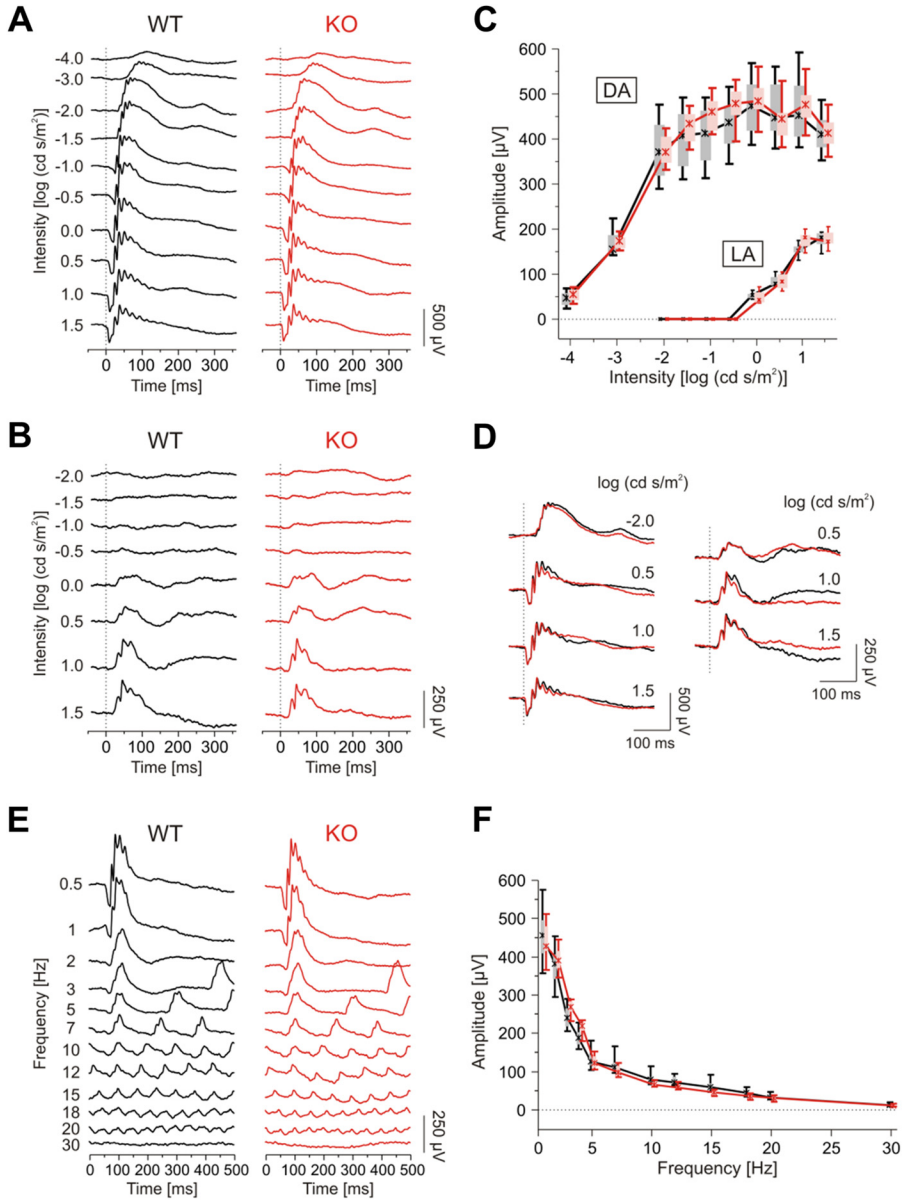

FIGURE 4. ***In vivo* functional analysis in *Pde6h*$^{-/-}$ mice using ERG.** *A–D*, dark-adapted (*A*) and light-adapted (*B*) single-flash ERG intensity series of a representative WT and P*de6h*$^{-/-}$ (KO) mouse. Quantitative evaluation (box-and-whisker plot, indicating 5th, 25th, 50th, 75th, 95th percentiles of the data) of b-wave amplitudes of WT (*black*) and *Pde6h*$^{-/-}$ (*red*) mice under dark-adapted (*DA*) and light-adapted (*LA*) conditions (*C*). The amplitude data are plotted as a function of the logarithm of the flash intensity. Overlay of a set of response traces of WT (*black*) and *Pde6h*$^{-/-}$ (*red*) mice (*D*) (*left column* from *A* and *right column* from *B*). *E* and *F*, flicker ERG frequency series at a fixed stimulus intensity of 0.5 log cd s/m^2 of a representative WT and *Pde6h*$^{-/-}$ mouse (*E*). Quantitative evaluation of flicker amplitudes in each group (*F*) (boxes-and-whisker plot and color code as above). The amplitude data are plotted as a function of the stimulus frequency. Comparison of ERG data from WT ($n = 4$) and *Pde6h*$^{-/-}$ mice ($n = 4$) was performed at 4–5 months of age. There was no difference between both groups.

mined. As expected, the quantification demonstrated that the PDE6H fluorescence signal was absent from the cone outer segments of *Pde6h*$^{-/-}$ upon labeling the retina with PDE6H-specific antibody (Fig. 5, *A* and *B*). In contrast, labeling of the *Pde6h* null retina with a common PDE6G/H antibody resulted in significant fluorescence signals in the cone photoreceptors (Fig. 5, *D* and *E*). Indeed, the relative amount of cone fluorescence in the *Pde6h*$^{-/-}$ and WT retina was similar upon labeling the photoreceptors with PDE6G/H antibody. We conclude from this finding that the usually "rod-specific" PDE6G protein is present in cones, thereby preventing catalytic deregulation of PDE6, which would otherwise cause cone dysfunction and/or degeneration. This finding is further supported by immunoblotting analysis of retina lysates derived from WT and *Pde6h*$^{-/-}$ mice showing no differences in the total PDE6G plus PDE6H protein levels (Fig. 5*F*) and control samples of recombinant PDE6H protein to determine the specificity of the antibodies (Fig. 5, *F* and *G*).

DISCUSSION

To study the molecular pathomechanisms of visual dysfunction, in particular cone dystrophies and ACHM *in vivo*, we generated mice in which the inhibitory subunit of cone photoreceptor *Pde6h* was genetically deleted. Based on previous findings from different gene-targeted mouse models (17, 23, 25, 43) and human patients, we expected the loss of PDE6H func-

tion to result in deregulated PDE6 activity and thereby impaired cone signal transduction and photoreceptor loss. However, neither our immunohistochemical labeling of photoreceptors using different cone and rod markers (Figs. 2 and 5) nor *in vivo* analyses by SLO and OCT imaging (Fig. 3, *D* and *E*) revealed any degenerative processes or morphological alterations in *Pde6h*$^{-/-}$ retinae. Importantly, M- and S-opsin expression was distributed normally throughout the *Pde6h*-deficient

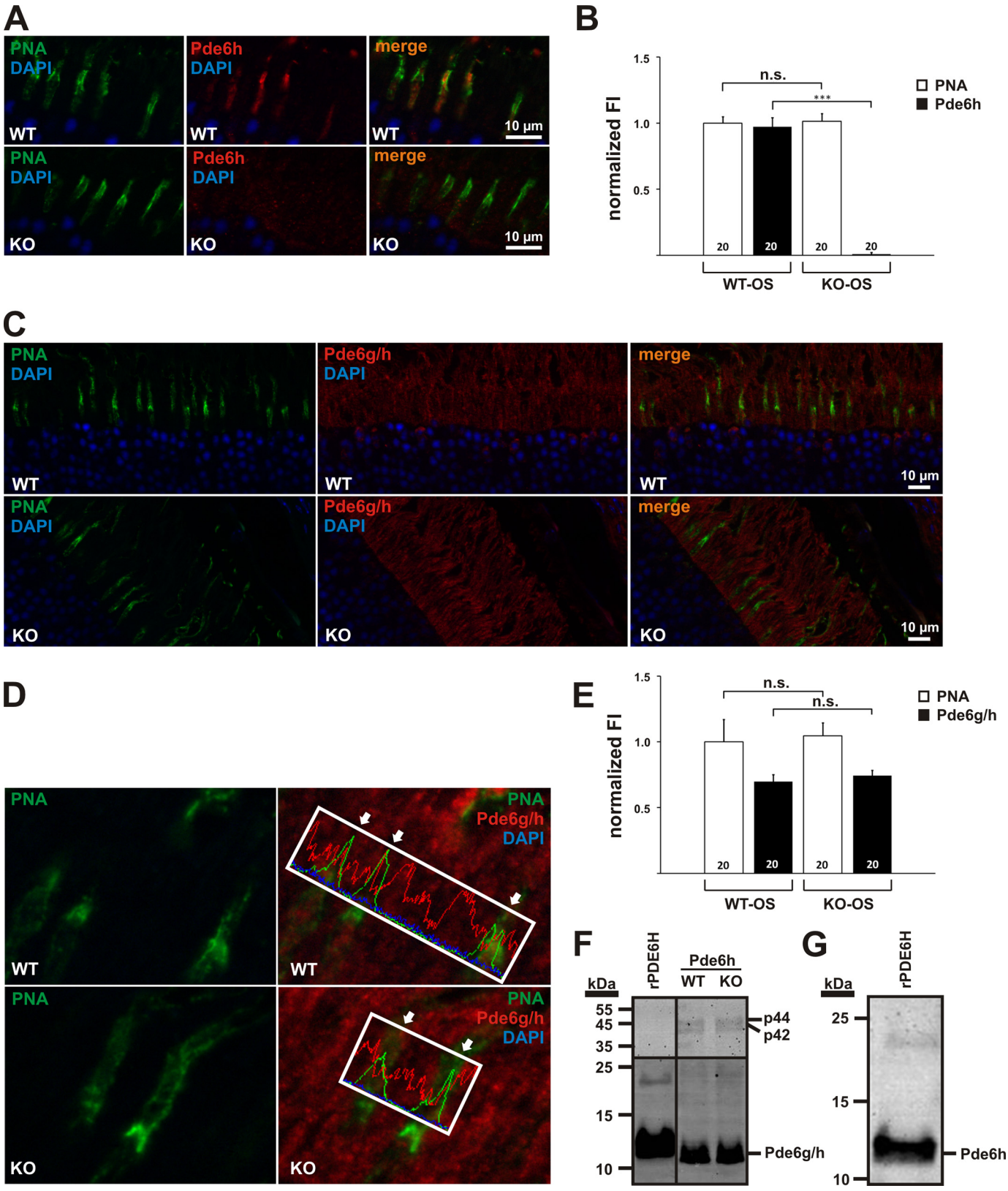

photoreceptor cell layer (Fig. 3, *B* and *C*), although we confirmed the absence of PDE6H in these cells. To assess the retinal function of *Pde6h*$^{-/-}$ mice *in vivo*, we performed a set of ERG analyses (Fig. 4). Light- and dark-adapted measurements and different stimulus conditions were tested to investigate discrete rod or cone functions as well as mixed rod and cone responses. In contrast to the patients with a nonsense mutation in *PDE6H* that suffer from incomplete ACHM due to severely reduced cone functions (28), we did not find any signs of distorted photoreceptor function in *Pde6h*$^{-/-}$ ERGs at all applied stimuli (Fig. 4). Importantly, retinal signaling after single-flash stimulation in dark-adapted and light-adapted flash ERGs as well as the dynamic properties by repetitively stimulating the retina in flicker ERGs were not different between *Pde6h*$^{-/-}$ and WT mice. Together, these findings identify important species-to-species differences for the roles of mouse *Pde6h* and human *PDE6H.* Murine *Pde6h* is either dispensable for visual signal transduction in cones or the chronic lack of PDE6H may be efficiently substituted by PDE6G *in vivo* in mice.

The presence of rod- and cone-specific isoforms for the various components of the phototransduction signaling cascade is fairly conserved in vertebrate species. The exclusivity of their expression in either rods or cones and thus the primary impairment of one of the two types of photoreceptors upon gene ablation have been demonstrated in numerous animal models. However, there are several important exceptions in which species-specific differences in gene expression or the phenotypic presentation of mutants has been reported. For instance, *GRK1* and *GRK7* are considered to encode the G-protein receptor kinases that phosphorylate the photopigment during the photoresponse shut-off in rods and cones, respectively. Immunohistological analysis revealed prominent differences in the expression of GRK1 and GRK7 in rods and cones between species (47, 48). Moreover, mutations in *GRK1* in humans causes Oguchi disease, a hereditary form of night blindness with a marked decrease in rod response and recovery kinetics (49, 50), whereas ablation of *Grk1* in the mouse results in equally impaired light response and recovery kinetics in both rods and cones (51, 52). Similarly, differences between man and mouse were reported for retinal photoreceptor guanylate cyclases (GC-E and GC-F) and the interacting guanylate cyclase activator proteins 1–3 (5, 6, 53). Indeed, the distribution and expression levels of these important factors vary a lot between species; hence, rearrangements made upon disruption of a single guanylate cyclase or guanylate cyclase activator proteins may result in rather unique phenotypes. For example, GCAP1 and GCAP2 expression levels in rod and cone photoreceptors differ between a number of species, and GCAP3 is expressed exclusively in human and zebrafish cones but is not detectable in mice (54–57). In the rod-dominated rat and mouse retinae, the outer segment layer shows uniform GC-E immunoreactivity (58, 59), whereas in monkey and human retinae, GC-E labeling of cones seems to be more intense than in rod outer segments (58, 60, 61). In contrast to human GC-F that is present in photoreceptor cell bodies and inner segments (54, 62), murine GC-F is largely restricted to cone OS (53). Distinct expression patterns for GC-E and GC-F imply cross-species differences in the development, function, and/or survival of photoreceptors when one or the other isoform is functionally impaired or eliminated. Indeed, recessive mutations in the human GC-E gene (*GUCY2D*) are known to cause Leber's congenital amaurosis type 1 (Table 1), an early onset rod/cone dystrophy with severe early onset visual impairment (63). GC-E-deficient mice, however, develop cone dystrophy with rods remaining morphologically intact maintaining light responsiveness (64). Along the same lines, mutations in the *GCAP1* gene have been associated with an autosomal dominant form of cone dystrophy in human patients (65–67), whereas expression of GCAP1 in the *Gcap1/Gcap2*-deficient mouse rescues rod photoreceptor response in this mutant (68).

We find it very unlikely that deregulated cGMP degrading activity of the catalytic PDE6 subunits in cones can be tolerated by the cone photoreceptor. Indeed, the available data from mutant zebrafish, the *cpfl1* mutant mouse model that carries a spontaneous mutation in the catalytic subunit of cone phosphodiesterase (*i.e. Pde6c*), and from humans with mutations within the *PDE6C* gene (25, 69) point toward the importance of a tightly regulated PDE6 in cones. Reduced PDE6C activity interferes with the visual signal transduction process thereby causing cone dysfunction, photoreceptor degeneration, and ACHM (25). Because our genetic approach to inactivate *Pde6h* revealed no retinal phenotype, we tested for potential compensatory mechanisms and found strong evidence for expression of the rod-specific PDE6G protein in cones of *Pde6h*$^{-/-}$ mice (Fig. 5). For dichromatic mice, this finding suggests that PDE6G may effectively participate in cone PDE6 regulation to allow accurate visual signal transduction even in the absence of functional PDE6H.

Our data are in good agreement with several reports that found a reciprocal substitution of the catalytic PDE6 subunits in rod and cone photoreceptors. Kolandaivelu *et al.* (70) gener-

FIGURE 5. **Analysis of rod PDE6G expression in *Pde6h*$^{-/-}$ cones by double immunofluorescence labeling.** *A,* co-labeling of mouse WT and *Pde6h*$^{-/-}$ (*KO*) retina sections with a PDE6H-specific antibody (*red*, 1:1000) and peanut hemagglutinin (PNA-FITC, *green*, 1:100) as a cone marker. Co-localization of PDE6H and PNA was detectable in WT but not in *Pde6h*$^{-/-}$ retina. *B,* measurement of relative fluorescence intensities was performed for 20 cone OS of each genotype for PDE6H and PNA. Only coordinates that were positive for PNA (*green, cones*) were considered for the quantification. As expected, *Pde6h*$^{-/-}$ outer segments revealed no PDE6H fluorescence, PNA immunoreactivity of cones, however, was similar between genotypes. *C* and *D,* co-labeling of mouse WT and *Pde6h*$^{-/-}$ retina sections with PNA-FITC (*green*, 1:100) as cone marker and an antibody staining both PDE6G and PDE6H protein (*red,* 1:1000) in lower (*C*) and at a higher magnification (*D*). DAPI was used as a nucleus-staining fluorochrome. *C,* single channel (*left, middle*) and multichannel (*right*) panels are displayed. *D,* peaks of PNA-FITC fluorescence intensity in histograms (*boxes*) were used to identify the localization of cones. At these coordinates (*arrows*), relative fluorescence intensities for PDE6G/H (*red*) and PNA (*green*) were digitally measured in *grayscale* and quantified as shown in *E*. Only coordinates that are positive for PNA (*green, cones*) were analyzed for PDE6G/H (and PDE6H) fluorescence intensities (*red*). Data were normalized to background fluorescence. *E*, measurement of relative fluorescence intensities was performed for 20 cone OS. *Pde6h*$^{-/-}$ outer segments revealed PDE6G/H immunoreactivity, suggesting that rod PDE6G is present in *Pde6h*$^{-/-}$ cones. *F*, Western blot analysis of PDE6G/H protein of WT and *Pde6h*$^{-/-}$ retinae. Heterologously expressed recombinant PDE6H protein (*rPDE6H*) serves as a positive control. *Pde6h*$^{-/-}$ retina showed no reduction in total PDE6G/H protein levels compared with WT retina. *G*, specificity of the PDE6H antibody was validated with recombinant PDE6H (rPDE6H) by immunoblotting. *B* and *E*, *n.s.* indicates non-significant difference between groups; ***, $p < 0.001$.

TABLE 1
Exemplary gene-targeted mouse models failing to produce a phenotype like in humans

Gene (human/mouse ortholog)	Human disease	Phenotype of gene-targeted mouse model	Ref.
Neuro-sensory system			
CLN2/Cln2	Neuronal ceroid lipofuscinoses (NCL)	Several neuronal characteristics of NCL are resembled by the gene-targeted $Cln2^{-/-}$ model, but no retinal degeneration has been reported	75
CLRN1/Clrn1	Usher syndrome type3 (USH3)	Like USH3 patients, $Clrn1^{-/-}$ mice develop deafness, but they do not show a retinal phenotype	76
CRB1/Crb1	Retinitis pigmentosa (RP12), Leber congenital amaurosis (LCA8)	$Crb1^{-/-}$ mutant mice develop local morphological disorganization of the retina but visual function remains unaffected	77
MYO7A/Myo7a	Usher syndrome type1 (USH1B)	Mutations in the murine orthologous gene lead to cochlear and vestibular dysfunction but not to retinal defects	78
GUCY2D/Gucy2e	Leber congenital amaurosis type1 (LCA1)	Cone responses in $Gucy2e^{-/-}$ mice are undetectable, but morphologically normal rods show paradoxical behavior in their responses to light, whereas human patients present with rod/cone dystrophy	31, 64
RDH12/Rdh12	Leber congenital amaurosis (LCA13)	Retinal homogenates from Rdh12-deficient mice exhibit markedly decreased capacity to reduce exogenous retinaldehydes *in vitro*. Furthermore, the bisretinoid compound diretinoid-pyridinium-ethanolamine (A2E) is increased in Rdh12-deficient mice of various genetic backgrounds. However, mutant mice do not show a retinal degeneration phenotype	79, 80
RPGR/Rpgr	Retinitis pigmentosa (RP3)	Mutations in RPGR lead to severe retinal dystrophy in humans and dogs. However, mouse models null for RPGR have only a very mild phenotype compared with those observed in XlRP3-affected humans and dogs	81
ZNS			
TGIF1/Tgif1	Holoprosencephaly-4	In contrast to human patients, homozygous null mice present no congenital malformations and are viable and fertile	82
OCRL1/Ocrl1	Oculocerebrorenal syndrome of Lowe	Murine null mutants show no apparent phenotype possibly due to a functional compensation by *Inpp5b*	83

ated a model to study ACHM in the absence of rods. The authors produced double-mutant neural retina leucine zipper ($Nrl^{-/-}$) and *cpfl1* mice that develop a so-called "all cone-like" retina aiming to study the functional consequences of depleted cone *Pde6c* catalytic subunits. ERG measurements of $Nrl^{-/-}$/*cpfl1* double mutants lacked, as expected, rod activity, but surprisingly showed S-cone-mediated responses under light-adapted conditions. Moreover, immunoblotting of $Nrl^{-/-}$/*cpfl1* retinae revealed the presence of cone PDE6H and rod PDE6G suggesting that the PDE6G protein is normally expressed in murine cones (70). In addition to the inhibitory PDE6 proteins, catalytic rod PDE6 subunits were detectable in cone photoreceptors of the all cone-like retina model. Based on these data and results from this study, we conclude that the configuration of the multisubunit enzyme PDE6 is functionally more interchangeable than previously thought. It was shown that the catalytic cone subunit PDE6C by assembling with the inhibitory PDE6G subunit of rods can restore rod functions in the rod *Pde6b*-deficient *rd10* mouse model (71). Because the catalytic domains of PDE6 are highly conserved among rods and cones, it is not surprising that they may substitute for each other (70–73).

Interestingly, Siegert *et al.* (74) created a transcriptional code and disease map for retinal cell types allowing for a quantitative comparison of gene expression across different cell types in the adult mouse retina. The expression data reveal the presence of "rod-specific" *Pde6g* in mouse rods and cones, whereas *Pde6h* is exclusively expressed in cones (74) strongly supporting our own findings in the $Pde6h^{-/-}$ model (Figs. 2 and 5). However, the lack of *Pde6g* causes severe and progressive loss of photoreceptor cells leading to early retinal degeneration. Accordingly, the ERG of $Pde6g^{-/-}$ mice shows an age-dependent severely diminished response in both a- and b-wave components and became almost undetectable after 3 months (23) strongly supporting the unique role of *Pde6g* in the retina. In this regard, it was not important for the outcome whether the *Pde6g* gene was chronically depleted or acutely knocked down (43).

The prominent changes in photopic and flicker-ERG responses observed in the patients with a *PDE6H* nonsense mutation indicated an important but not compensable role for the inhibitory γ-subunit in cone visual signal transduction in humans (24). This mutation gives rise to a strongly shortened (by more than 85% of its total length) PDE6H protein most likely representing a functional null allele because conserved domains relevant for transducin binding (29, 30) and inhibition of the catalytic activity of PDE6 are missing. We conclude that human cone PDE6 activity is highly vulnerable to changes in the photoreceptor signaling network and that the human retina lacks back-up mechanisms for the regulation of cone PDE6 activity.

Similar to the disparity described in this study, differences in the phenotype seen in human patients and that of the corresponding mouse mutant (*e.g.* knockouts generated by gene targeting) are well documented for retinal diseases as well as disorders of other organs (see Table 1 for a brief selection). Such cross-species differences hamper studies into the pathophysiology of disease and the development and evaluation of therapies that rely on the availability of proper animal models. On the other hand such examples provide excellent opportunities to study the flexibility and modularity of redundant systems in terms of evolutionary adaptation.

Acknowledgments—We thank Stephen Tsang for discussions; Brigitte Pfeiffer-Guglielmi for providing the GlyPhos antibody; Johannes Wilbertz from the Karolinska Center for Transgene Technologies (Stockholm) for performing blastocyst injections; and Marc Freichel from the Institute of Pharmacology in Heidelberg for providing Cre deleter mice.

REFERENCES

1. Burns, M. E., and Arshavsky, V. Y. (2005) Beyond counting photons: trials and trends in vertebrate visual transduction. *Neuron* **48,** 387–401
2. Kawamura, S., and Tachibanaki, S. (2008) Rod and cone photoreceptors: molecular basis of the difference in their physiology. *Comp. Biochem. Physiol A. Mol. Integr. Physiol.* **150,** 369–377
3. Biel, M., and Michalakis, S. (2009) Cyclic nucleotide-gated channels. *Handb. Exp. Pharmacol.* **191,** 111–136
4. Nickle, B., and Robinson, P. R. (2007) The opsins of the vertebrate retina: insights from structural, biochemical, and evolutionary studies. *Cell. Mol. Life Sci.* **64,** 2917–2932
5. Karan, S., Frederick, J. M., and Baehr, W. (2010) Novel functions of photoreceptor guanylate cyclases revealed by targeted deletion. *Mol. Cell. Biochem.* **334,** 141–155
6. Palczewski, K., Sokal, I., and Baehr, W. (2004) Guanylate cyclase-activating proteins: structure, function, and diversity. *Biochem. Biophys. Res. Commun.* **322,** 1123–1130
7. Wen, X. H., Dizhoor, A. M., and Makino, C. L. (2014) Membrane guanylyl cyclase complexes shape the photoresponses of retinal rods and cones. *Front. Mol. Neurosci.* **7,** 45
8. Zhang, X., and Cote, R. H. (2005) cGMP signaling in vertebrate retinal photoreceptor cells. *Front. Biosci.* **10,** 1191–1204
9. Muradov, K. G., Granovsky, A. E., Schey, K. L., and Artemyev, N. O. (2002) Direct interaction of the inhibitory γ-subunit of rod cGMP phosphodiesterase (PDE6) with the PDE6 GAFa domains. *Biochemistry* **41,** 3884–3890
10. Gillespie, P. G., and Beavo, J. A. (1988) Characterization of a bovine cone photoreceptor phosphodiesterase purified by cyclic GMP-Sepharose chromatography. *J. Biol. Chem.* **263,** 8133–8141
11. Shimizu-Matsumoto, A., Itoh, K., Inazawa, J., Nishida, K., Matsumoto, Y., Kinoshita, S., Matsubara, K., and Okubo, K. (1996) Isolation and chromosomal localization of the human cone cGMP phosphodiesterase γ cDNA (PDE6H). *Genomics* **32,** 121–124
12. Arshavsky, V. Y., and Burns, M. E. (2012) Photoreceptor signaling: supporting vision across a wide range of light intensities. *J. Biol. Chem.* **287,** 1620–1626
13. Hofmann, F., Bernhard, D., Lukowski, R., and Weinmeister, P. (2009) cGMP regulated protein kinases (cGK). *Handb. Exp. Pharmacol.* **191,** 137–162
14. Kemp-Harper, B., and Schmidt, H. H. (2009) cGMP in the vasculature. *Handb. Exp. Pharmacol.* **191,** 447–467
15. Kleppisch, T., and Feil, R. (2009) cGMP signalling in the mammalian brain: role in synaptic plasticity and behaviour. *Handb. Exp. Pharmacol.* **191,** 549–579
16. Lev, S. (2001) Molecular aspects of retinal degenerative diseases. *Cell. Mol. Neurobiol.* **21,** 575–589
17. Bowes, C., Li, T., Danciger, M., Baxter, L. C., Applebury, M. L., and Farber, D. B. (1990) Retinal degeneration in the rd mouse is caused by a defect in the β subunit of rod cGMP-phosphodiesterase. *Nature* **347,** 677–680
18. Gal, A., Orth, U., Baehr, W., Schwinger, E., and Rosenberg, T. (1994) Heterozygous missense mutation in the rod cGMP phosphodiesterase β-subunit gene in autosomal dominant stationary night blindness. *Nat. Genet.* **7,** 551
19. Ferrari, S., Di Iorio, E., Barbaro, V., Ponzin, D., Sorrentino, F. S., and Parmeggiani, F. (2011) Retinitis pigmentosa: genes and disease mechanisms. *Curr. Genomics* **12,** 238–249
20. McLaughlin, M. E., Ehrhart, T. L., Berson, E. L., and Dryja, T. P. (1995) Mutation spectrum of the gene encoding the β subunit of rod phosphodiesterase among patients with autosomal recessive retinitis pigmentosa. *Proc. Natl. Acad. Sci. U.S.A.* **92,** 3249–3253
21. Huang, S. H., Pittler, S. J., Huang, X., Oliveira, L., Berson, E. L., and Dryja, T. P. (1995) Autosomal recessive retinitis pigmentosa caused by mutations in the α subunit of rod cGMP phosphodiesterase. *Nat. Genet.* **11,** 468–471
22. Dvir, L., Srour, G., Abu-Ras, R., Miller, B., Shalev, S. A., and Ben-Yosef, T. (2010) Autosomal recessive early-onset retinitis pigmentosa caused by a mutation in PDE6G, the gene encoding the γ subunit of rod cGMP phosphodiesterase. *Am. J. Hum. Genet.* **87,** 258–264
23. Tsang, S. H., Gouras, P., Yamashita, C. K., Kjeldbye, H., Fisher, J., Farber, D. B., and Goff, S. P. (1996) Retinal degeneration in mice lacking the γ subunit of the rod cGMP phosphodiesterase. *Science* **272,** 1026–1029
24. Grau, T., Artemyev, N. O., Rosenberg, T., Dollfus, H., Haugen, O. H., Cumhur Sener, E., Jurklies, B., Andreasson, S., Kernstock, C., Larsen, M., Zrenner, E., Wissinger, B., and Kohl, S. (2011) Decreased catalytic activity and altered activation properties of PDE6C mutants associated with autosomal recessive achromatopsia. *Hum. Mol. Genet.* **20,** 719–730
25. Chang, B., Grau, T., Dangel, S., Hurd, R., Jurklies, B., Sener, E. C., Andreasson, S., Dollfus, H., Baumann, B., Bolz, S., Artemyev, N., Kohl, S., Heckenlively, J., and Wissinger, B. (2009) A homologous genetic basis of the murine cpfl1 mutant and human achromatopsia linked to mutations in the PDE6C gene. *Proc. Natl. Acad. Sci. U.S.A.* **106,** 19581–19856
26. Kohl, S., Baumann, B., Rosenberg, T., Kellner, U., Lorenz, B., Vadalà, M., Jacobson, S. G., and Wissinger, B. (2002) Mutations in the cone photoreceptor G-protein α-subunit gene GNAT2 in patients with achromatopsia. *Am. J. Hum. Genet.* **71,** 422–425
27. Kohl, S., Varsanyi, B., Antunes, G. A., Baumann, B., Hoyng, C. B., Jägle, H., Rosenberg, T., Kellner, U., Lorenz, B., Salati, R., Jurklies, B., Farkas, A., Andreasson, S., Weleber, R. G., Jacobson, S. G., *et al.* (2005) CNGB3 mutations account for 50% of all cases with autosomal recessive achromatopsia. *Eur. J. Hum. Genet.* **13,** 302–308
28. Kohl, S., Coppieters, F., Meire, F., Schaich, S., Roosing, S., Brennenstuhl, C., Bolz, S., van Genderen, M. M., Riemslag, F. C., European Retinal Disease Consortium, Lukowski, R., den Hollander, A. I., Cremers, F. P., De Baere, E., Hoyng, C. B., and Wissinger, B. (2012) A nonsense mutation in PDE6H causes autosomal recessive incomplete achromatopsia. *Am. J. Hum. Genet.* **91,** 527–532
29. Slep, K. C., Kercher, M. A., He, W., Cowan, C. W., Wensel, T. G., and Sigler, P. B. (2001) Structural determinants for regulation of phosphodiesterase by a G protein at 2.0 A. *Nature* **409,** 1071–1077
30. Artemyev, N. O., Rarick, H. M., Mills, J. S., Skiba, N. P., and Hamm, H. E. (1992) Sites of interaction between rod G-protein α-subunit and cGMP-phosphodiesterase γ-subunit. Implications for the phosphodiesterase activation mechanism. *J. Biol. Chem.* **267,** 25067–25072
31. Hamilton, S. E., and Hurley, J. B. (1990) A phosphodiesterase inhibitor specific to a subset of bovine retinal cones. *J. Biol. Chem.* **265,** 11259–11264
32. Schwenk, F., Baron, U., and Rajewsky, K. (1995) A cre-transgenic mouse strain for the ubiquitous deletion of loxP-flanked gene segments including deletion in germ cells. *Nucleic Acids Res.* **23,** 5080–5081
33. Leiss, V., Friebe, A., Welling, A., Hofmann, F., and Lukowski, R. (2011) Cyclic GMP kinase I modulates glucagon release from pancreatic α-cells. *Diabetes* **60,** 148–156
34. Lukowski, R., Rybalkin, S. D., Loga, F., Leiss, V., Beavo, J. A., and Hofmann, F. (2010) Cardiac hypertrophy is not amplified by deletion of cGMP-dependent protein kinase I in cardiomyocytes. *Proc. Natl. Acad. Sci. U.S.A.* **107,** 5646–5651
35. Leiss, V., Illison, J., Domes, K., Hofmann, F., and Lukowski, R. (2014) Expression of cGMP-dependent protein kinase type I in mature white adipocytes. *Biochem. Biophys. Res. Commun.* **452,** 151–156
36. Lukowski, R., Weinmeister, P., Bernhard, D., Feil, S., Gotthardt, M., Herz, J., Massberg, S., Zernecke, A., Weber, C., Hofmann, F., and Feil, R. (2008) Role of smooth muscle cGMP/cGKI signaling in murine vascular restenosis. *Arterioscler. Thromb. Vasc. Biol.* **28,** 1244–1250
37. Pfeiffer-Guglielmi, B., Francke, M., Reichenbach, A., Fleckenstein, B., Jung, G., and Hamprecht, B. (2005) Glycogen phosphorylase isozyme pattern in mammalian retinal Muller (glial) cells and in astrocytes of retina and optic nerve. *Glia* **49,** 84–95
38. Nihira, M., Anderson, K., Gorin, F. A., and Burns, M. S. (1995) Primate rod and cone photoreceptors may differ in glucose accessibility. *Invest. Ophthalmol. Vis. Sci.* **36,** 1259–1270
39. Sahaboglu, A., Paquet-Durand, O., Dietter, J., Dengler, K., Bernhard-Kurz, S., Ekström, P. A., Hitzmann, B., Ueffing, M., and Paquet-Durand, F. (2013) Retinitis pigmentosa: rapid neurodegeneration is governed by slow cell death mechanisms. *Cell Death Dis.* **4,** e488
40. Tanimoto, N., Sothilingam, V., and Seeliger, M. W. (2013) Functional phenotyping of mouse models with ERG. *Methods Mol. Biol.* **935,** 69–78

41. Fischer, M. D., Huber, G., Beck, S. C., Tanimoto, N., Muehlfriedel, R., Fahl, E., Grimm, C., Wenzel, A., Remé, C. E., van de Pavert, S. A., Wijnholds, J., Pacal, M., Bremner, R., and Seeliger, M. W. (2009) Noninvasive, *in vivo* assessment of mouse retinal structure using optical coherence tomography. *PLoS One* **4,** e7507
42. Seeliger, M. W., Beck, S. C., Pereyra-Muñoz, N., Dangel, S., Tsai, J. Y., Luhmann, U. F., van de Pavert, S. A., Wijnholds, J., Samardzija, M., Wenzel, A., Zrenner, E., Narfström, K., Fahl, E., Tanimoto, N., Acar, N., and Tonagel, F. (2005) *In vivo* confocal imaging of the retina in animal models using scanning laser ophthalmoscopy. *Vis. Res.* **45,** 3512–3519
43. Liu, J., Timmers, A. M., Lewin, A. S., and Hauswirth, W. W. (2005) Ribozyme knockdown of the γ-subunit of rod cGMP phosphodiesterase alters the ERG and retinal morphology in wild-type mice. *Invest. Ophthalmol. Vis. Sci.* **46,** 3836–3844
44. Szél, A., Röhlich, P., Caffé, A. R., Juliusson, B., Aguirre, G., and Van Veen, T. (1992) Unique topographic separation of two spectral classes of cones in the mouse retina. *J. Comp. Neurol.* **325,** 327–342
45. Applebury, M. L., Antoch, M. P., Baxter, L. C., Chun, L. L., Falk, J. D., Farhangfar, F., Kage, K., Krzystolik, M. G., Lyass, L. A., and Robbins, J. T. (2000) The murine cone photoreceptor: a single cone type expresses both S and M opsins with retinal spatial patterning. *Neuron* **27,** 513–523
46. Tanimoto, N., Muehlfriedel, R. L., Fischer, M. D., Fahl, E., Humphries, P., Biel, M., and Seeliger, M. W. (2009) Vision tests in the mouse: Functional phenotyping with electroretinography. *Front. Biosci.* **14,** 2730–2737
47. Chen, C. K., Zhang, K., Church-Kopish, J., Huang, W., Zhang, H., Chen, Y. J., Frederick, J. M., and Baehr, W. (2001) Characterization of human GRK7 as a potential cone opsin kinase. *Mol. Vis.* **7,** 305–313
48. Weiss, E. R., Ducceschi, M. H., Horner, T. J., Li, A., Craft, C. M., and Osawa, S. (2001) Species-specific differences in expression of G-protein-coupled receptor kinase (GRK) 7 and GRK1 in mammalian cone photoreceptor cells: implications for cone cell phototransduction. *J. Neurosci.* **21,** 9175–9184
49. Yamamoto, S., Sippel, K. C., Berson, E. L., and Dryja, T. P. (1997) Defects in the rhodopsin kinase gene in the Oguchi form of stationary night blindness. *Nat. Genet.* **15,** 175–178
50. Miyake, Y., Horiguchi, M., Suzuki, S., Kondo, M., and Tanikawa, A. (1996) Electrophysiological findings in patients with Oguchi's disease. *Jpn. J. Ophthalmol.* **40,** 511–519
51. Lyubarsky, A. L., Chen, C., Simon, M. I., and Pugh, E. N., Jr. (2000) Mice lacking G-protein receptor kinase 1 have profoundly slowed recovery of cone-driven retinal responses. *J. Neurosci.* **20,** 2209–2217
52. Chen, C. K., Burns, M. E., Spencer, M., Niemi, G. A., Chen, J., Hurley, J. B., Baylor, D. A., and Simon, M. I. (1999) Abnormal photoresponses and light-induced apoptosis in rods lacking rhodopsin kinase. *Proc. Natl. Acad. Sci. U.S.A.* **96,** 3718–3722
53. Baehr, W., Karan, S., Maeda, T., Luo, D. G., Li, S., Bronson, J. D., Watt, C. B., Yau, K. W., Frederick, J. M., and Palczewski, K. (2007) The function of guanylate cyclase 1 and guanylate cyclase 2 in rod and cone photoreceptors. *J. Biol. Chem.* **282,** 8837–8847
54. Imanishi, Y., Li, N., Sokal, I., Sowa, M. E., Lichtarge, O., Wensel, T. G., Saperstein, D. A., Baehr, W., and Palczewski, K. (2002) Characterization of retinal guanylate cyclase-activating protein 3 (GCAP3) from zebrafish to man. *Eur. J. Neurosci.* **15,** 63–78
55. Kachi, S., Nishizawa, Y., Olshevskaya, E., Yamazaki, A., Miyake, Y., Wakabayashi, T., Dizhoor, A., and Usukura, J. (1999) Detailed localization of photoreceptor guanylate cyclase activating protein-1 and -2 in mammalian retinas using light and electron microscopy. *Exp. Eye Res.* **68,** 465–473
56. Otto-Bruc, A., Fariss, R. N., Haeseleer, F., Huang, J., Buczyłko, J., Surgucheva, I., Baehr, W., Milam, A. H., and Palczewski, K. (1997) Localization of guanylate cyclase-activating protein 2 in mammalian retinas. *Proc. Natl. Acad. Sci. U.S.A.* **94,** 4727–4732
57. Cuenca, N., Lopez, S., Howes, K., and Kolb, H. (1998) The localization of guanylyl cyclase-activating proteins in the mammalian retina. *Invest. Ophthalmol. Vis. Sci.* **39,** 1243–1250
58. Cooper, N., Liu, L., Yoshida, A., Pozdnyakov, N., Margulis, A., and Sitaramayya, A. (1995) The bovine rod outer segment guanylate cyclase, *ROS-GC,* is present in both outer segment and synaptic layers of the retina. *J. Mol. Neurosci.* **6,** 211–222
59. Haire, S. E., Pang, J., Boye, S. L., Sokal, I., Craft, C. M., Palczewski, K., Hauswirth, W. W., and Semple-Rowland, S. L. (2006) Light-driven cone arrestin translocation in cones of postnatal guanylate cyclase-1 knockout mouse retina treated with AAV-GC1. *Invest. Ophthalmol. Vis. Sci.* **47,** 3745–3753
60. Dizhoor, A. M., Lowe, D. G., Olshevskaya, E. V., Laura, R. P., and Hurley, J. B. (1994) The human photoreceptor membrane guanylyl cyclase, RetGC, is present in outer segments and is regulated by calcium and a soluble activator. *Neuron* **12,** 1345–1352
61. Liu, X., Seno, K., Nishizawa, Y., Hayashi, F., Yamazaki, A., Matsumoto, H., Wakabayashi, T., and Usukura, J. (1994) Ultrastructural localization of retinal guanylate cyclase in human and monkey retinas. *Exp. Eye Res.* **59,** 761–768
62. Shyjan, A. W., de Sauvage, F. J., Gillett, N. A., Goeddel, D. V., and Lowe, D. G. (1992) Molecular cloning of a retina-specific membrane guanylyl cyclase. *Neuron* **9,** 727–737
63. Perrault, I., Rozet, J. M., Calvas, P., Gerber, S., Camuzat, A., Dollfus, H., Châtelin, S., Souied, E., Ghazi, I., Leowski, C., Bonnemaison, M., Le Paslier, D., Frézal, J., Dufier, J. L., Pittler, S., Munnich, A., and Kaplan, J. (1996) Retinal-specific guanylate cyclase gene mutations in Leber's congenital amaurosis. *Nat. Genet.* **14,** 461–464
64. Yang, R. B., Robinson, S. W., Xiong, W. H., Yau, K. W., Birch, D. G., and Garbers, D. L. (1999) Disruption of a retinal guanylyl cyclase gene leads to cone-specific dystrophy and paradoxical rod behavior. *J. Neurosci.* **19,** 5889–5897
65. Downes, S. M., Holder, G. E., Fitzke, F. W., Payne, A. M., Warren, M. J., Bhattacharya, S. S., and Bird, A. C. (2001) Autosomal dominant cone and cone-rod dystrophy with mutations in the guanylate cyclase activator 1A gene-encoding guanylate cyclase activating protein-1. *Arch. Ophthalmol.* **119,** 96–105
66. Wilkie, S. E., Li, Y., Deery, E. C., Newbold, R. J., Garibaldi, D., Bateman, J. B., Zhang, H., Lin, W., Zack, D. J., Bhattacharya, S. S., Warren, M. J., Hunt, D. M., and Zhang, K. (2001) Identification and functional consequences of a new mutation (E155G) in the gene for GCAP1 that causes autosomal dominant cone dystrophy. *Am. J. Hum. Genet.* **69,** 471–480
67. Payne, A. M., Downes, S. M., Bessant, D. A., Taylor, R., Holder, G. E., Warren, M. J., Bird, A. C., and Bhattacharya, S. S. (1998) A mutation in guanylate cyclase activator 1A (GUCA1A) in an autosomal dominant cone dystrophy pedigree mapping to a new locus on chromosome 6p21.1. *Hum. Mol. Genet.* **7,** 273–277
68. Howes, K. A., Pennesi, M. E., Sokal, I., Church-Kopish, J., Schmidt, B., Margolis, D., Frederick, J. M., Rieke, F., Palczewski, K., Wu, S. M., Detwiler, P. B., and Baehr, W. (2002) GCAP1 rescues rod photoreceptor response in GCAP1/GCAP2 knockout mice. *EMBO J.* **21,** 1545–1554
69. Stearns, G., Evangelista, M., Fadool, J. M., and Brockerhoff, S. E. (2007) A mutation in the cone-specific *pde6* gene causes rapid cone photoreceptor degeneration in zebrafish. *J. Neurosci.* **27,** 13866–13874
70. Kolandaivelu, S., Chang, B., and Ramamurthy, V. (2011) Rod phosphodiesterase-6 (PDE6) catalytic subunits restore cone function in a mouse model lacking cone PDE6 catalytic subunit. *J. Biol. Chem.* **286,** 33252–33259
71. Deng, W. T., Sakurai, K., Kolandaivelu, S., Kolesnikov, A. V., Dinculescu, A., Li, J., Zhu, P., Liu, X., Pang, J., Chiodo, V. A., Boye, S. L., Chang, B., Ramamurthy, V., Kefalov, V. J., and Hauswirth, W. W. (2013) Cone phosphodiesterase-6α′ restores rod function and confers distinct physiological properties in the rod phosphodiesterase-6β-deficient rd10 mouse. *J. Neurosci.* **33,** 11745–11753
72. Muradov, H., Boyd, K. K., and Artemyev, N. O. (2010) Rod phosphodiesterase-6 PDE6A and PDE6B subunits are enzymatically equivalent. *J. Biol. Chem.* **285,** 39828–39834
73. Muradov, H., Boyd, K. K., Haeri, M., Kerov, V., Knox, B. E., and Artemyev, N. O. (2009) Characterization of human cone phosphodiesterase-6 ectopically expressed in *Xenopus laevis* rods. *J. Biol. Chem.* **284,** 32662–32669
74. Siegert, S., Cabuy, E., Scherf, B. G., Kohler, H., Panda, S., Le, Y. Z., Fehling, H. J., Gaidatzis, D., Stadler, M. B., and Roska, B. (2012) Transcriptional code and disease map for adult retinal cell types. *Nat. Neurosci.* **15,** 487–495

75. Sleat, D. E., Wiseman, J. A., El-Banna, M., Kim, K. H., Mao, Q., Price, S., Macauley, S. L., Sidman, R. L., Shen, M. M., Zhao, Q., Passini, M. A., Davidson, B. L., Stewart, G. R., and Lobel, P. (2004) A mouse model of classical late-infantile neuronal ceroid lipofuscinosis based on targeted disruption of the CLN2 gene results in a loss of tripeptidyl-peptidase I activity and progressive neurodegeneration. *J. Neurosci.* **24,** 9117–9126
76. Geller, S. F., Guerin, K. I., Visel, M., Pham, A., Lee, E. S., Dror, A. A., Avraham, K. B., Hayashi, T., Ray, C. A., Reh, T. A., Bermingham-McDonogh, O., Triffo, W. J., Bao, S., Isosomppi, J., Västinsalo, H., *et al.* (2009) CLRN1 is nonessential in the mouse retina but is required for cochlear hair cell development. *PLoS Genet.* **5,** e1000607
77. van de Pavert, S. A., Kantardzhieva, A., Malysheva, A., Meuleman, J., Versteeg, I., Levelt, C., Klooster, J., Geiger, S., Seeliger, M. W., Rashbass, P., Le Bivic, A., and Wijnholds, J. (2004) Crumbs homologue 1 is required for maintenance of photoreceptor cell polarization and adhesion during light exposure. *J. Cell Sci.* **117,** 4169–4177
78. el-Amraoui, A., Sahly, I., Picaud, S., Sahel, J., Abitbol, M., and Petit, C. (1996) Human Usher 1B/mouse shaker-1: the retinal phenotype discrepancy explained by the presence/absence of myosin VIIA in the photoreceptor cells. *Hum. Mol. Genet.* **5,** 1171–1178
79. Maeda, A., Maeda, T., Sun, W., Zhang, H., Baehr, W., and Palczewski, K. (2007) Redundant and unique roles of retinol dehydrogenases in the mouse retina. *Proc. Natl. Acad. Sci. U.S.A.* **104,** 19565–19570
80. Chrispell, J. D., Feathers, K. L., Kane, M. A., Kim, C. Y., Brooks, M., Khanna, R., Kurth, I., Hübner, C. A., Gal, A., Mears, A. J., Swaroop, A., Napoli, J. L., Sparrow, J. R., and Thompson, D. A. (2009) Rdh12 activity and effects on retinoid processing in the murine retina. *J. Biol. Chem.* **284,** 21468–21477
81. Mavlyutov, T. A., Zhao, H., and Ferreira, P. A. (2002) Species-specific subcellular localization of RPGR and RPGRIP isoforms: implications for the phenotypic variability of congenital retinopathies among species. *Hum. Mol. Genet.* **11,** 1899–1907
82. Shen, J., and Walsh, C. A. (2005) Targeted disruption of Tgif, the mouse ortholog of a human holoprosencephaly gene, does not result in holoprosencephaly in mice. *Mol. Cell. Biol.* **25,** 3639–3647
83. Jänne, P. A., Suchy, S. F., Bernard, D., MacDonald, M., Crawley, J., Grinberg, A., Wynshaw-Boris, A., Westphal, H., and Nussbaum, R. L. (1998) Functional overlap between murine Inpp5b and Ocrl1 may explain why deficiency of the murine ortholog for OCRL1 does not cause Lowe syndrome in mice. *J. Clin. Invest.* **101,** 2042–2053